Bioactive Materials 6 (2021) 2400–2411

Contents lists available at ScienceDirect

Bioactive Materials

journal homepage: www.sciencedirect.com/journal/bioactive-materials

Bilayer dissolving microneedle array containing 5-fluorouracil and triamcinolone with biphasic release profile for hypertrophic scar therapy

Beibei Yang [a], Yating Dong [a], Yifeng Shen [a], Ailin Hou [a], Guilan Quan [b,**], Xin Pan [a,*], Chuanbin Wu [b]

[a] School of Pharmaceutical Sciences, Sun Yat-sen University, Guangzhou, 510006, China
[b] College of Pharmacy, Jinan University, Guangzhou, 510632, China

ARTICLE INFO

Keywords:
Hypertrophic scar
Bilayer microneedle
Biphasic release
Triamcinolone acetonide
5-Fluorouracil

ABSTRACT

Hypertrophic scar (HS) is an undesirable skin abnormality following deep burns or operations. Although intralesional multi-injection with the suspension of triamcinolone acetonide (TA) and 5-fluorouracil (5-Fu) has exhibited great promise to HS treatment in clinical, the difference of metabolic behavior between TA and 5-Fu remarkably compromised the treatment efficacy. Besides, the traditional injection with great pain is highly dependent on the skill of the experts, which results in poor compliance. Herein, a bilayer dissolving microneedle (BMN) containing TA and 5-Fu (TA-5-Fu-BMN) with biphasic release profile was designed for HS therapy. Equipped with several micro-scale needle tips, the BMN could be self-pressed into the HS with uniform drug distribution and less pain. Both *in vitro* permeation and *in vivo* HS retention tests revealed that TA and 5-Fu could coexist in the scar tissue for a sufficient time period due to the well-designed biphasic release property. Subsequently, the rabbit ear HS model was established to assess therapeutic efficacy. The histological analysis showed that TA-5-Fu-BMN could significantly reduce abnormal fibroblast proliferation and collagen fiber deposition. It was also found that the value of scar elevation index was ameliorated to a basal level, together with the downregulation of mRNA and protein expression of Collagen I (Col I) and transforming growth factor-β1 (TGF-β1) after application of TA-5-Fu-BMN. In conclusion, the BMN with biphasic release profiles could serve as a potential strategy for HS treatment providing both convenient administrations as well as controlled drug release behavior.

1. Introduction

Hypertrophic scars (HS) are abnormal tissues often occurring after deep trauma, intensive burn injury, or large-wound surgical operations. The patients with excessive scars usually face a series of physical, psychological, and cosmetic problems because of the symptoms of pain, pruritus, and skin stiffness [1–4]. The main reasons for HS formation are related to hypertrophic scar fibroblast (HSFb) over-proliferation and excessive deposition of collagen [2,5,6]. Up to now, various therapies are developed for the treatment of HS, including surgical excision, laser therapy, radiotherapy, silicon material compression, and intralesional corticosteroid injection [7,8]. Problems associated with these therapeutic modalities remain unsolved, such as high recurrence rate after surgery or laser therapy, serious side effects of radiotherapy, and long-term use of pressure therapy [9,10]. Currently, the application of corticosteroids has achieved tremendous progress in this field, specifically the intralesional injection of triamcinolone acetonide (TA), which is the most frequently used and effective technique, through inhibiting fibroblast growth and collagen synthesis [11]. Nevertheless, various undesirable glucocorticoid side effects usually occur after injection with high-dose TA alone, such as tissue atrophy, pain, and changes in pigmentation [12]. These issues have critically limited further development and application of TA. Thus, there is an extremely urgent need to explore an alternative strategy for HS therapy [13].

5-Fluorouracil (5-Fu), an extensively used pyrimidine analog, is also promising in anti-scarring application owing to its significant effect on inhibiting DNA synthesis [14,15]. Despite these advances, its efficacy as a monotherapy for treating HS still needs further investigation, because

Peer review under responsibility of KeAi Communications Co., Ltd.
* Corresponding author.
** Corresponding author.
E-mail addresses: quanguilan@jnu.edu.cn (G. Quan), panxin2@mail.sysu.edu.cn (X. Pan).

https://doi.org/10.1016/j.bioactmat.2021.01.014
Received 31 October 2020; Received in revised form 26 December 2020; Accepted 17 January 2021

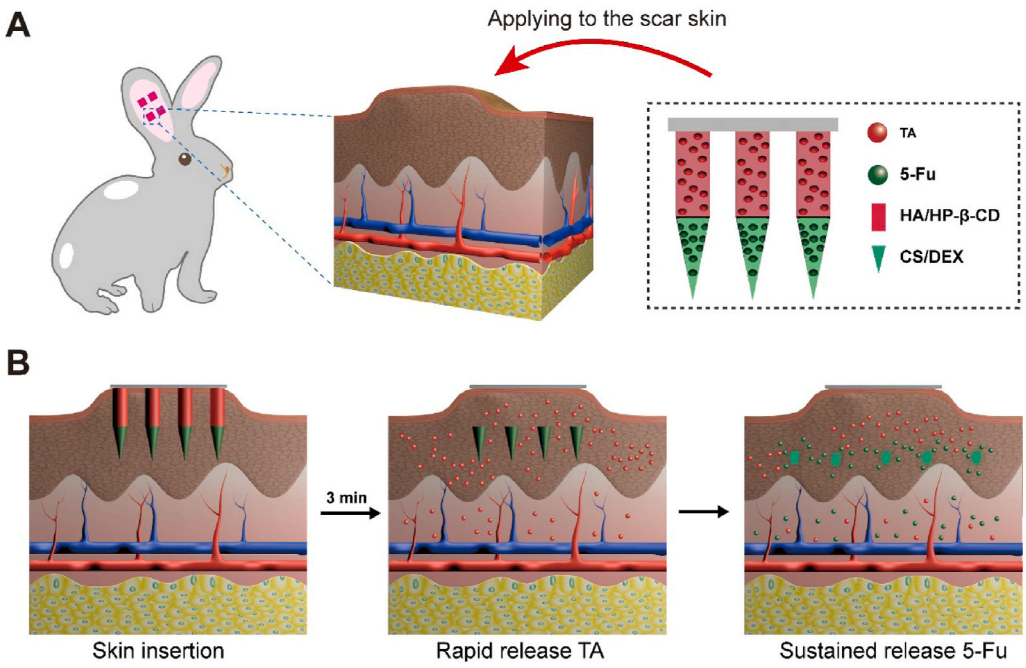

Scheme 1. Schematic illustration of HS model in rabbit ear, the design of the BMN with 5-Fu in the tip layer and TA in the tail layer of the needle (A), and drug delivery with biphasic release profile to scar lesion using BMN for synergic HS treatment (B).

it may cause leukopenia and thrombocytopenia [16]. Previous studies have demonstrated that combining TA with 5-Fu could potentiate each other, resulting in superior therapeutic efficacy for HS treatment, while offering better safety with fewer adverse reactions [5].

At present, the main administration route for HS therapy is intralesional multi-injection using conventional needles to penetrate the scar tissue, which is a highly invasive way causing severe pain and poor patient compliance, and also requires skilled person for operation [17]. Besides, topical multi-injection tends to burst release drugs in a short period, thus frequent administrations are required for the treatment of long-term diseases like HS, which increases the risk of infection. According to previous studies, as one of the most widely used modalities in HS therapy, the treatment interval of TA has a range of 2–6 weeks, while 5-Fu needs to be intralesionally injected once, twice, even three times a week [18]. Because 5-Fu can be easily eliminated by endogenous dihydropyrimidine dehydrogenase in tissues, resulting in short retention time [19]. Due to the different metabolic behavior between TA and 5-Fu in the skin, the actual retention time of the two drugs after combined administration is greatly disparate, which may compromise the therapeutic efficiency. Therefore, the design of a reasonable drug delivery system containing 5-Fu and TA with improved bioavailability is still a great challenge in HS therapy. A localized and easy-to-use drug delivery system with controlled release profile and good patient compliance is highly preferred.

Microneedle (MN) patch, which is a micrometer-scale medical device, has attracted considerable attention as an effective transdermal drug delivery system [20–22]. Through directly penetrating the skin and creating reversible microchannels with less pain, MN can significantly improve the transdermal drug delivery efficiency [23–25]. Equipped with several needle tips, the MN can provide uniform drug distribution in the HS site due to the well-designed structure. Moreover, MN can allow patients to self-administer, which brings great convenience [26,27]. Collectively, MN is an attractive alternative to conventional intralesional multi-injection [28,29]. However, conventional MN seldom concerns the retention behavior of different drugs. To address this issue, bilayer MN (BMN) with biphasic release properties was expected to realize better co-delivery.

This study aimed to design a bilayer MN to control the drug release profile of different drugs for efficient HS treatment. Specifically, the needle tip layer was fabricated by chitosan (CS) and dextran (DEX), which was used to slowly release 5-Fu. The needle tail layer was composed of hyaluronic acid (HA) as the excipient and hydroxypropyl-beta-cyclodextrin (HP-β-CD) as the inclusion compound of insoluble TA, which was used for rapid release of TA (Scheme 1). The characteristics of the fabricated BMN including physical morphology, mechanical strength, insertion ability, *in vitro* drug release profile, and *in vivo* drug retention were investigated. The *in vivo* pharmacodynamic study showed that the therapeutic ability of two drugs could potentiate each other by constructing the BMN with biphasic release properties, which provides a new idea for the efficient treatment of HS.

2. Materials and methods

2.1. Materials

Triamcinolone acetonide (TA, purity>99.5%), 5-Fluorouracil (5-Fu, purity>99.5%), absolute alcohol, propanetriol, acetic acid, and triethanolamine were obtained from Aladdin (Shanghai, China). Polydimethylsiloxane (PDMS, Sylgard 184) was purchased from Dow Corning (Shanghai, China). Hyaluronic acid (HA, M_W = 10,000 Da) was purchased from Bloomage Freda Biopharm Co., Ltd. (Shanxi, China). Dextran (DEX, M_W = 40,000 Da), chitosan (CS, 95% degree of polymerization, M_W = 400,000 Da), and trypan blue were obtained from Aladdin (Shanghai, China). HP-β-CD (M.S. = 4.44, M_W = 1391 Da) was purchased from Xi'an Deli Biopharm Co., Ltd. (Shanxi, China). Polyvinyl pyrrolidone (PVP K90) was kindly donated by BASF (Ludwigshafen, Germany). Human HSFb was obtained from Shanghai Baili Biotechnology Co., Ltd. (Shanghai, China). Dulbecco's Modified Eagle Medium/Nutrient Mixture F-12 (DMEM/F-12) was obtained from Gibco (Shanghai, China). Fetal bovine serum (FBS) was purchased from Hangzhou Sijiqing Bioengineering Materials Co., Ltd. (Hangzhou, China). Dimethyl sulfoxide (DMSO) was obtained from MP Biomedicals (Shanghai, China). Cell Counting Kit-8 (CCK-8) was purchased from Dojindo Molecular Technologies, Inc. (Kyushu, Japan). TA injection and 5-Fu injection were respectively obtained from Shanghai Xudong Haipu Pharmaceutical Co., Ltd. (Shanghai, China) and Kunming Jida

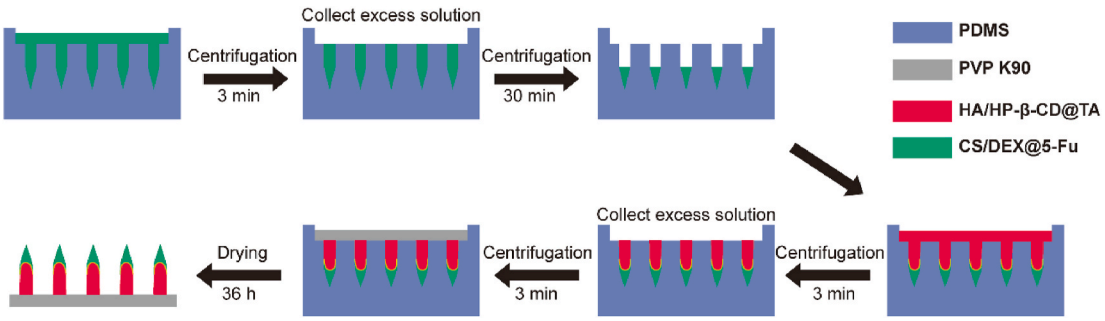

Fig. 1. Schematic illustration of the fabrication process for BMN.

Pharmaceutical Co., Ltd. (Kunming, China). Paraformaldehyde was obtained from Biosharp Life Science Co., Ltd. (Anhui, China). The materials and reagents used in Real-time Quantitative PCR Analysis and Western Blotting Analysis were offered by Servicebio (Hubei, China). All the other solvents and materials used were of analytical reagent grade.

2.2. Fabrication of molds

The brass master mold was fabricated by a micro-milling technique based on the precise design by computer, which was consisted of 144 (12 × 12) microneedles with a tip-to-tip space of 800 μm. Each needle was 300 μm in width and 1200 μm in height, including a square prism (600 μm in height) and a pyramidal needle tip (600 μm in height). The female molds were precisely obtained by inversely replicating the master mold. After pouring PDMS solution over the master mold and allowing it to cure at 80 °C for 2 h, the PDMS female molds were peeled off and repeatedly used for microneedle fabrication in this study [30].

2.3. Preparation of matrix material for microneedles

CS was added in 1% acetic acid solution (5%, w/v) and constantly stirred until the solution was clear. And 1 g of DEX was dissolved in 2 mL of deionized water. Then, these solutions were mixed at a ratio of 1:1 (v/v) under stirring at room temperature. A defined amount of 5-Fu was dissolved into the above solution to form the matrix material for the tips of BMN, followed by placing it at room temperature for 30 min to remove bubbles in the solution.

Next, excess TA was added to the HP-β-CD solution (2:5, w/v) and stirred for 5 h. The inclusion compound (IC) was collected by centrifugation to remove the excess TA precipitation. The needle tail matrix was obtained by adding HA to the IC solution at a ratio of 1:2 (w/v).

2.4. Design and fabrication of BMN

A three-step casting procedure was used to fabricate the blank BMN array (Fig. 1). Briefly, CS/DEX solution (200 μL) was poured over the PDMS mold and centrifuged at 4000 rpm for 3 min at 5 °C to completely fill the mold cavities. The excess solution remaining on the surface of the mold was removed for later use. The mold was centrifuged again at the same speed and temperature for 30 min to dry the needle tips. Then, the HA/HP-β-CD solution was added onto the PDMS mold and centrifuged under the same condition for 3 min. After removal of the excess solution, approximately 200 μL of PVP K90 ethanol solution (30%, w/v) was cast onto each mold and centrifuged for another 3 min. The filled mold was dried in a desiccator for 36 h at room temperature to ultimately obtain the blank BMN patch.

The CS/DEX@5-Fu solution was used as the needle tip layer solution, HA/HP-β-CD@TA solution was used as the needle tail layer solution and drug-loaded BMN (TA-5-Fu-BMN) was prepared according to the above three-step centrifugation method. Similarly, the blank tip layer solution (CS/DEX) and HA/HP-β-CD@TA solution were centrifuged into the mold step by step to prepare BMN containing TA alone (TA-BMN). CS/DEX@5-Fu solution and blank needle tail layer solution (HA/HP-β-CD) were used to prepare BMN containing 5-Fu alone (5-Fu-BMN). The same amount of 5-Fu and HA/HP-β-CD@TA solution were mixed to obtain the drug-loaded tail layer BMN (Tail layer@TA-5-Fu-BMN).

HPLC was used to determine the drug loading in BMN. The obtained BMN was observed by using a scanning electron microscope (SEM, JSM-6330F, Jeol, Tokyo, Japan) and a stereo fluorescence microscope (SteREO Lumar V12, Zeiss, Germany) [31]. To visually observe the drug distribution in the microneedles, the fluorescent probes fluorescein isothiocyanate (FITC) and rhodamine B (RhB) were used to replace 5-Fu and TA, respectively. The obtained fluorescent BMN was imaged by a confocal laser scanning microscope (CLSM, LSM710, Zeiss, Germany).

2.5. Mechanical performance of BMN

The texture analyzer (CT3, Brookfield, USA) was used to investigate the mechanical strength of the BMN [32,33]. Briefly, a single patch of blank BMN and drug-loaded BMN was placed on the metal platform and pressed by a pressure probe at a constant speed of 0.1 mm/s. Once the tip of the microneedle touched the pressure sensor, the testing machine subsequently recorded a function of the force and distance in the computer.

Using the same texture analyzer, the isolated fresh rabbit ear HS tissue was fixed on the rigid stainless-steel platform to investigate the penetration force of BMN. Meanwhile, the BMN was attached vertically to the pressure probe using double-sided tape, with the needles directed downward. During the movement of the probe, the forces were recorded when the uppermost tip of BMN touched the scarred skin, and a function of pressure and the displacement distance was also recorded, as shown in Fig. 3A.

2.6. In vitro insertion capability of BMN

To assess the *in vitro* skin insertion capability, the drug-loaded BMN patch was pressed onto the SD rat dorsal skin in a vertical direction for 3 min. After peeling off the BMN, 0.4% trypan blue solution was immediately used to stain the insertion site for 2 min [34]. Then the stained skin was imaged under an optical microscope (ECLIPSE Ts2, Nikon, Japan). To observe the histological section, the inserted skin was fixed in 4% paraformaldehyde, embedded in paraffin, sliced into 5 μm sections, and followed by staining with hematoxylin and eosin (H&E).

To further intuitively observe the insertion depth in the skin, optical coherence tomography (OCT) microscope (Michelson Diagnostics Ltd., Kent, UK) was used to obtain real-time images of the insertion process. The laser wavelength of the OCT system was set as 1310 nm. Finally, the acquired images were analyzed using Image J software (National Institutes of Health, Bethesda, USA) to determine the insertion depth.

2.7. In vitro drug permeation study

The permeation kinetics of TA and 5-Fu across HS tissue were performed *in vitro* using the Franz Cell diffusion chamber (TK-24BL, Shanghai Kaikai Technology Trade Co., Ltd, China) with a permeation area of approximately 1.8 cm^2. The receptor compartment was filled with 8 mL of PBS (pH 6.2) maintained at 37 °C and magnetically stirred at 250 rpm. First, the excised HS tissue was fixed on the diffusion cell with the dermal side faced the receptor chamber [35]. Then, TA-5-Fu BMN, Tail layer@TA-5-Fu BMN were pressed onto the rabbit ear HS skin for 3 min ($n = 3$). The samples were withdrawn at predetermined time intervals (10 min, 20 min, 40 min, 1 h, 2 h, 3 h, 6 h, 9 h, 12 h, 24 h, 48 h, 72 h, 96 h, 120 h) and replaced with an equal volume of fresh PBS. Commercially available 5-Fu injection and TA injection containing an equivalent amount of drug were injected into the skin as a comparison ($n = 3$). The samples were filtered through a 0.22 μm microporous membrane, and the amount of TA and 5-Fu in the receptor was determined by HPLC, respectively. The mobile phase for 5-Fu assay consisted of PBS (pH 3.5) and methanol (95:5, v/v), and the effluent was monitored at an ultraviolet–visible (UV) absorption wavelength of 265 nm. For TA determination, the mobile phase was constituted of acetonitrile and distilled water (60:40, v/v), with monitoring at a UV absorption wavelength of 240 nm. Calibration curves of 5-Fu and TA were linear over the concentration range of 2.5–75 μL/mL and 2–120 μL/mL, respectively. The cumulative permeation amount was calculated according to the following formula:

$$Q_n = \left[C_n V + \sum_{i=1}^{n-1} C_i V_i \right] \quad (1)$$

Where C_n represented the measured drug concentration of the nth sampling, C_i was the concentration measured for each sampling, V represented the volume of the receptor medium, V_i represented the volume of each sampling, and Q_n is the cumulative amount of drug.

2.8. In vivo drug retention

Nine New Zealand rabbits after the completion of HS model were anesthetized with Su Mian Xin II (0.05 mL/kg) and Zoletil 50 (0.15 mL/kg). TA-5-Fu-BMN and Tail layer@TA-5-Fu BMN ($n = 3$) were punctured into the scarred skin for 3 min and then covered with medical tape. The commercial TA-5-Fu injection was also applied as a comparison. After administration at 0 min, 20 min, 40 min, 1 h, 2 h, 4 h, 24 h, and 72 h, the scar tissue was collected, and the drug that remained on the scar surface was wiped off using the cotton balls containing alcohol. The excised scar was cut into pieces, followed by adding 2 mL of HPLC-grade methanol and homogenization to extract the drug from the scar. Subsequently, the sample was vortexed for 3 min and sonicated for another 30 min. After centrifugation at 5000 rpm for 5 min at 4 °C, the supernatant was collected, filtered with 0.22 μm microporous membrane, and assayed by HPLC.

2.9. In vitro cell proliferation assay

Human HSFb were incubated in DMEM/F-12 containing 10% FBS in a humidified incubator (3110, Thermo Fisher Scientific, USA) at 37 °C with 5% CO_2. Subsequently, 5.0×10^3 cells were seeded into each well in 96-well plates and cultured for 24 h. One hundred milligram of TA was dissolved in 0.8 mL of DMSO and then diluted with serum-containing medium to 8 groups (300.0, 200.0, 100.0, 50.0, 25.0, 12.5, 5.0, 3.0 μg/mL). A series of 5-Fu solutions at the same concentration gradients were also prepared only with serum-containing medium. Then the cell medium was replaced with 100 μL of samples and the cells treated with the pure medium were used as the control. After incubation for 24 h, a CCK-8 cell proliferation-toxicity detection kit was used to detect cell viability at 490 nm. *Cell viability* was calculated according to the following equation:

$$Cell\ viability\ (\%) = [(A_s - A_b) / (A_c - A_b)] \times 100\% \quad (2)$$

Where, A_s represents the absorbance of the cells in experimental groups, A_b represents the absorbance of the medium only containing CCK-8 without cells, Ac represents the absorbance of the cells in control groups.

2.10. Cytotoxicity of excipients

The cytotoxicity of the excipients including DEX, CS, HA, and HP-β-CD was evaluated against HSFb. Aseptic ultrapure water was used to prepare the blank needle tip layer CS/DEX solution, needle tail HA/HP-β-CD solution. DMEM/F-12 was used to dilute by 50, 100, and 150 times, respectively. The following procedures were coincident with those as described above and the cell viability was also calculated by equation (2).

2.11. Optimization proportion of TA combined with 5-fu

To investigate the optimum proportion of TA and 5-Fu, the cells were seeded and cultured in 96-well plates. One hundred milligram 5-Fu was dissolved by DMEM/F-12 supplemented with 10% FBS and diluted to the concentration of 5.0 μg/mL. A series of TA solutions with different concentrations were prepared. Then, TA solution was mixed with 5-Fu solution at different proportions (TA: 5-Fu = 30:1, 20:1, 15:1, 9:1, 6:1, 3:1, 1:1, 1:3, 1:6, 1:9, 1:15, 1:20, 1:30 w/w). For each well, 100 μL of drug solution was added to replace the old medium. After incubation for another 24 h, the CCK-8 kit was added, and the cell viability was calculated. To further assess the synergy effect of TA and 5-Fu, the combination index (CI) was calculated according to the following equation:

$$CI_{50} = \frac{(C)_T}{(C_{50})_T} + \frac{(C)_F}{(C_{50})_F} \quad (3)$$

In equation (3), $(C)_T$ and $(C)_F$ represent the respective concentration of TA and 5-Fu at IC50 values when they were used in combination. $(C_{50})_T$ and $(C_{50})_F$ represent the concentration of TA alone and 5-Fu alone at their *IC50* values, respectively. When the CI_{50} value is less than 1, it represents a synergistic effect. When the value is equal to 1, it represents an addictive effect, while the value is more than 1, it represents an antagonistic effect. Meanwhile, the corresponding IC_{50} values in each concentration were calculated by linear regression method using SPSS.

2. 12. In vitro wound scratch assay

The HSFb cells were seeded into 6-well plates at a density of 1.0×10^5 cells per well with 2.0 mL of DMEM/F-12 containing 10% FBS and allowed to attach till the cells reached 80–90%. Then, the sterile pipette tips were used to draw the scratch in the middle of the culture, and the cells scratched off were washed away with PBS. Drug solutions were prepared with DMEM/F-12 supplemented with 0.5% FBS, including 5-Fu (5.0 μg/mL), TA (5.0 μg/mL), the combination of TA and 5-Fu both at the concentration of 5.0 μg/mL. For each well, cells were fed by 2.0 mL of the sample solution to replace the old medium. The migration of cells was photographed by an inversion microscope at 0, 12, and 24 h. The area of the scratch was analyzed by Image J, and *the wound healing rate (WHR)* was calculated according to the following equation:

$$WHR(\%) = (A_0 - A_t)/A_0 \times 100\% \quad (4)$$

In equation (4), A_0 and A_t represent the area of scratch at 0 h and t h, respectively.

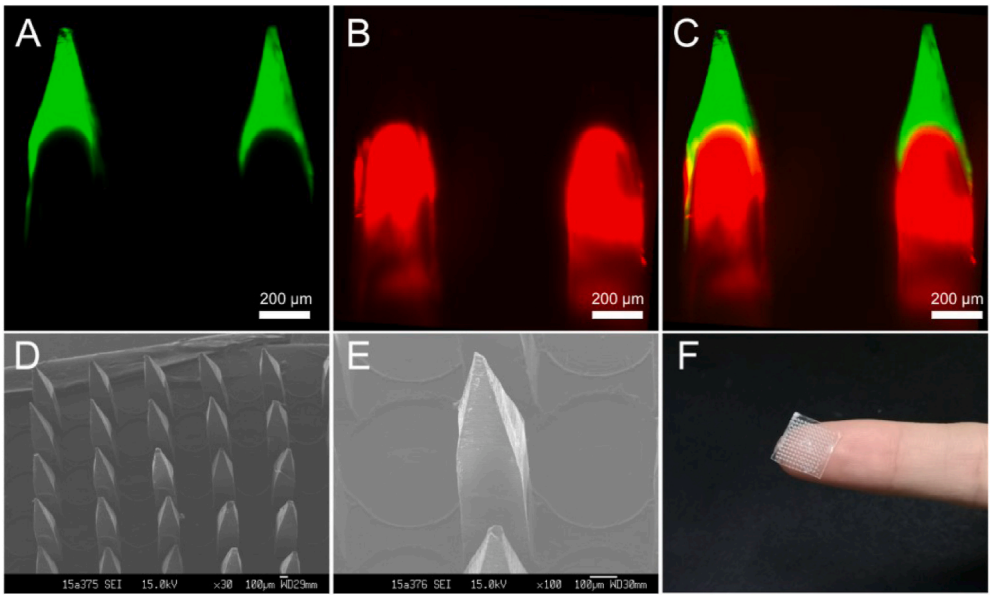

Fig. 2. Confocal micrographs of fluorescent BMN (A–C). FITC and RhB were shown as green fluorescence and red fluorescence, respectively; SEM images (D and E) and the photograph of BMN patch (F).

2.13. Pharmacodynamics studies

To evaluate the therapeutic efficacy of 5-Fu-TA-BMN *in vivo*, HS model was established in the rabbit ear [11,36]. The whole animal study was performed under the guidance of the Animal Ethical and Welfare Committee of Sun Yat-sen University (Approval No. SYSU-IACUC-2019-000275) and was under the National Institutes of Health and Nutrition Guidelines for the care and use of laboratory animals. Briefly, 24 New Zealand female rabbits weighing 1.5–2.0 kg were supplied by Guangdong Medical Experimental Animal Center (Guangdong, China). Four wounds (1 cm*1 cm) were created on the ventral surface of each ear, avoiding the central ear artery and marginal ear veins. Afterward, the full-thickness skin and perichondrium of each square were completely excised. After one week, the newly formed scab was removed to make the wound exposed again. After recovering and epithelializing for 22 days, the HS models were successfully established with a thickness ratio of more than 1.5 between HS tissue and normal skin.

All animals were randomly divided into seven groups ($n = 3$): blank control group (normal skin, NS), negative control group (HS), TA-5-Fu-injection group, drug-free BMN group, TA-BMN group, 5-Fu-BMN group, and TA-5-Fu-BMN group. No treatment was given in the NS group and the HS group. For the 5-Fu-TA injection group, 5-Fu injection and TA injection were mixed according to the clinical method and intralesionally multi-injected into the scar tissue using an insulin syringe at an angle of about 15° between the tip and the skin. The drug dose of the injection group was the same as that of the BMN. For the 5-Fu-BMN group, only 5-Fu was loaded at the needle tip. Similarly, for the TA-BMN group, only TA was loaded in the tail layer of the needle. The treatment was conducted on day 22, 29, and 36 after surgery, once a week for three consecutive weeks. For the MN groups (Drug-free BMN, TA-BMN, 5-Fu-BMN, and TA-5-Fu-BMN), the microneedle patches were pressed to the scar site for 3 min to detach the needle from the substrate. On Day 22 (before administration), Day 29 (one week after the first administration), Day 36 (one week after the second administration), and Day 43 (one week after the third administration), the HS tissues were collected for morphology observation, histological analysis, detection of mRNA and protein expression.

2.14. Efficacy evaluation and histological analysis

At each time point, 4 HS samples were collected randomly in each group for histological investigation, and normal skin was also collected as a control. The samples were fixed in 4% paraformaldehyde for 24 h, embedded in paraffin wax, and cross-sectioned along with the tissue. Then, H&E and Masson staining were performed to determine the re-epithelialization and collagen deposition extent, respectively [6,7]. The photographs of the staining samples were obtained using a camera EVOS FL Auto (Life Technologies Co., Ltd., USA) and analyzed by software Image J to calculate the *scar elevation index (SEI)* as follows:

$$SEI = H/H_0 \tag{5}$$

Where, H represents the length between the highest point to the surface of cartilage in HS, and H_0 represents the length from the stratum corneum to the surface of the cartilage at the bottom of HS.

2.15. Real-time quantitative PCR analysis

Total RNA was extracted from tissue samples using TRIzol reagent and the concentration, purity, and integrality of RNA were detected using a micro-spectrophotometer (NanoDrop2000, Thermo Fisher Scientific, USA). Then 1.5 μg of RNA from each sample was used to generate cDNA with Reverse Transcriptase M-MLV owning Olig (dT) 18 and random primer. Afterward, the cDNA was used for real-time quantitative PCR to measure type I collagen (Col-I) and transforming growth factor-beta1 (TGF-β1) expression with the specific primers. The amplification procedure was carried out in the designated order: 95 °C for 5 min, 39 circles of 95 °C for 10 s, and 60 °C for 34 s. Finally, Ct values were calculated based on the fluorescent signals, and the transcript standard was calculated using the $2^{-\Delta\Delta Ct}$ method. The specific oligonucleotide primers used for the PCR amplifications were as follows:

GAPDH: Forward primer: 5′-CCGCCCAGAACATCATCCCT-3’; Reverse primer: 5′-GCACTGTTGAAGTCGCAGGAGA-3’;

Col I: Forward primer: 5′-TGGTGAATCTGGACGTGAGGG-3’; Reverse primer: 5′- TTATGCCTCTGTCGCCCTGTT-3’

TGF-β1: Forward primer: 5′-CTGCTGTGGCTCCTAGTGTTGA-3’; Reverse primer: 5′-AGCCGCAGTTTGGACAGGAT-3’

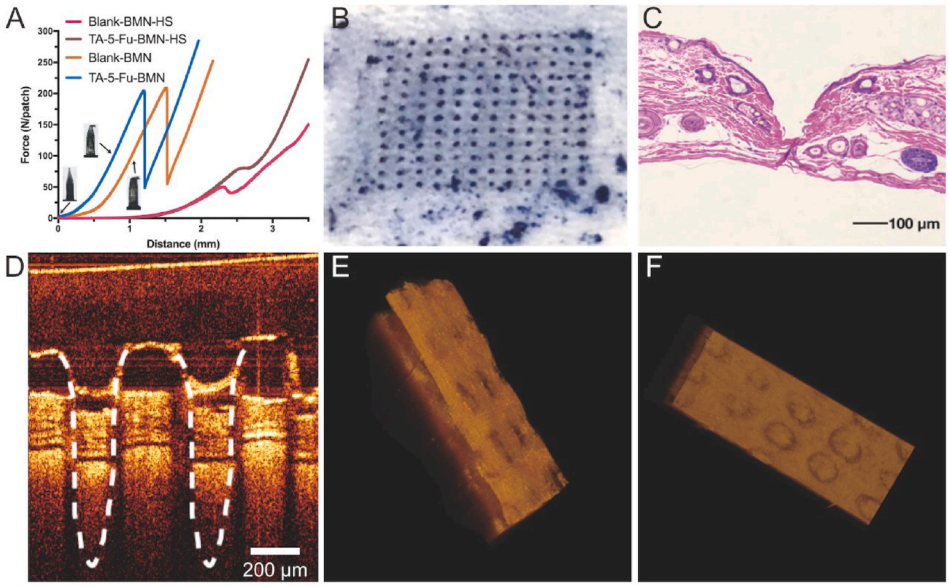

Fig. 3. The force curve of blank BMN and drug-loaded BMN analyzed by a texture analyzer (A); The photograph of the skin surface after insertion of BMN (B); Image of H&E-stained section of skin after the application of BMN (C); OCT image of insertion depth in the skin (D); Side view and top view after skin 3D reconstruction (E and F).

2.16. Western Blotting Analysis

The total proteins of each sample were extracted and measured by BCA protein quantitative kit. The proteins were separated with 10% sodium dodecyl sulfate-polyacrylamide gel electrophoresis (SDS-PAGE) loading buffer and then transferred to the PVDF membrane at 350 mA for 1 h. Subsequently, the PVDF membrane was blocked by 5% skimmed milk at room temperature for 2 h. Finally, the dilute solution (1:1000) of the primary antibody was added onto the membrane and incubated at room temperature for 2 h, followed by adding the dilute solution (1:2500) of the secondary antibody and incubation at room temperature for 1 h. The signals of proteins were normalized, and the expression change of the protein was determined using the corresponding GAPDH band. The gray value of each band was analyzed by Image J software for statistical analysis.

2.17. Statistical analysis

All data were expressed as mean ± standard deviation (SD). The statistical comparison was performed using a one-way analysis of variance (ANOVA) test after the normality test and variance homogeneity test using SPSS software. $P < 0.05$ was considered to be statistically significant.

3. Results and discussion

3.1. Preparation and characterization of BMN

The double-layered MN was prepared by a simple and mild three-step casting process (Fig. 1). As shown in Fig. 2A–C, the green fluorescence of FITC was mainly distributed at the needle tip layer, while the red fluorescence of RhB was shown at the tail layer of the microneedle. The layered structure was clear, which was consistent with the design expectation. The photomicrograph showed that the obtained BMN contained 144 (12*12) needles without any missing or broken phenomenon. The SEM images showed that the needles were uniformly arranged on the base substrate with consistent morphology. Each needle consisted of two parts, a square prism and a pyramidal needle tip (Fig. 2D and E).

3.2. Mechanical performance of BMN

Successful skin penetration is the prerequisite for effective transdermal drug delivery. Furthermore, HS has a denser tissue structure and thicker stratum corneum than normal skin. Thus, given the more hard and compact properties of HS, microneedles that can penetrate HS often require strong mechanical strength to effectively deliver drugs to subcutaneous tissues.

As shown in Fig. 3A, the curves of the BMN showed a sharp increase in force during the compression process. Subsequently, the microneedle broke and the force suddenly dropped down with the fracture force of approximately 200 N. Previous studies showed that the force required for each needle to penetrate the skin was less than 0.1 N [37], which indicated that the fabricated BMN in this study had sufficient mechanical strength to penetrate through the stratum corneum barrier without being broken. Moreover, it was found that the fracture force of the blank BMN and the drug-loaded BMN were similar, indicating that the mechanical strength of the microneedle was not affected after the addition of the drug.

The drug-loaded BMN and blank BMN were also applied to the HS scar at a speed of 0.1 mm/s. When the microneedle contacted the skin, the force began to slowly increase due to the elasticity of the skin. But after BMN was inserted into the skin, an instantaneous drop appeared on the curve followed by a constant increase. The inflection point on the curve represented the minimum force required to successfully penetrate the HS tissue. As shown in Fig. 3A, a force of 70 N was recorded when drug-loaded BMN penetrated through the skin. The fracture force of drug-loaded BMN (approximately 200 N) was far greater than 70 N, indicating that the obtained BMN possessed favorable mechanical strength to penetrate through the HS scar.

3.3. In vitro insertion capability of BMN

The proposed BMN was further applied to the rat dorsal skin to confirm the insertion capability. As shown in Fig. 3B, the rat skin surface showed an array of microholes (12*12) corresponding to the microneedle insertion sites, confirming that the obtained BMN was strong enough to break the skin barrier. Fig. 3C presented the histological section of the rat skin after BMN application. The deep cavities were clearly observed in the rat skin, which further confirming that the BMN

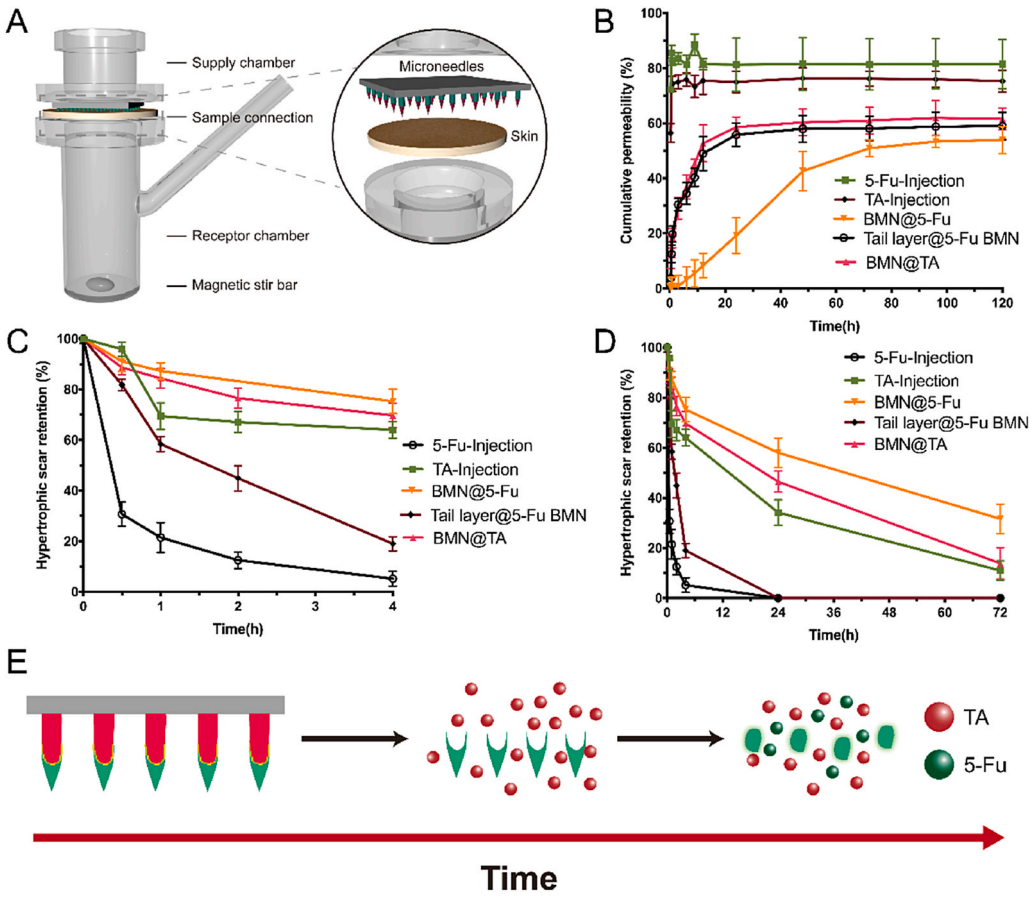

Fig. 4. Schematic illustration of the Franz diffusion cell model (A) and *ex-vivo* permeation profiles through rabbit HS from different formulations (B); HS retention of TA and 5-Fu at 4 h (C) and 72 h (D) of different formulations *in vivo*, respectively (mean ± SD, $n = 3$); Schematic illustration of drug release behavior from BMN (E).

could pierce through the stratum corneum and then be embedded into the skin. To further ascertain the penetration depth of BMN, a non-invasive technique, OCT, was used to obtain real-time images of the insertion process within 30 s. After the insertion of BMN, the microchannels created in the skin were shown in Fig. 3D and the whole shape of the BMN was maintained during the puncture process without fracture, indicating that the BMN had good rigidity. The 3D reconstruction was conducted to obtain the shape of the whole skin from the side and below view, respectively. As shown in Fig. 3E and F, visible and orderly holes could be seen, which also proved the successful penetration. The detectable signal could be up to 700 μm, which is inconsistent with the result obtained from the histological section. The possible reason was that the skin was shrunk during the preparation of the skin section for H&E staining. While OCT could detect the real-time signal after microneedle was embedded without causing skin deformation. Therefore, OCT was supposed to be a more persuasive strategy to measure the insertion depth of microneedle into the skin.

3.4. *In vitro drug permeation through HS tissue*

To investigate the permeation profile of encapsulated drugs, TA-5-Fu-BMN, Tail layer@TA-5-Fu BMN, and the TA-5-Fu mixed injection containing equivalent amounts of TA (52 μg) and 5-Fu (58 μg) were applied to the excised HS tissue and the cumulative drug permeation was monitored in Franz diffusion cells for 120 h (Fig. 4A). It was found that both TA and 5-Fu from mixed injection exhibited a burst release within 20 min (Fig. 4B), indicating that the majority of the drug was injected into the subcutaneous tissue layer during the use of syringes. Approximately 50% of both TA and 5-Fu in Tail layer@TA-5-Fu BMN, represented as Tail layer@TA BMN and Tail layer@5-Fu BMN, permeated through the HS tissue in 12 h. The permeation behavior was similar, indicating that the material of the microneedles was an important factor affecting the drug release rate. When 5-Fu was encapsulated in TA-5-Fu-BMN using CS and DEX as excipients, represented as BMN@5-Fu, the drug permeation rate slowed down with the cumulative permeation percentage was only 8.34 ± 4.51% at 12 h. The permeation rates of 5-Fu in the needle tip layer and tail layer were significantly different, which confirmed the successful construction of the bilayer microneedle co-administration system with biphasic release profile.

3.5. *In vivo drug retention*

The rabbit with HS model was used to investigate the drug metabolism and retention in the HS tissue. After the intralesional multi-injection of TA-5-Fu, the HS retention amount of 5-Fu, marked as 5-Fu-Injection in Fig. 4C and D, decreased sharply in 40 min, and could not be detected in tissue at 24 h after administration, indicating that 5-Fu was metabolized rapidly *in vivo* and could hardly remain in scar tissue to exert its efficacy. By contrast, TA administrated by injection, marked as TA-Injection in Fig. 4C and D, could stay in the HS for a long time since the metabolism rate of TA in the skin was slow, which was also consistent with previous studies. When these two drugs were injected together according to the clinical administration route, the action time for the combined effect was short, and the therapeutic efficiency was compromised because of the difference in the metabolic clearance rate. When encapsulating both 5-Fu and TA in the tail layer of BMN, marked as Tail layer@5-Fu BMN and Tail layer@TA BMN, the water-soluble HA quickly dissolved in the body fluid and released the drug. Then 5-Fu was rapidly metabolized, poorly improving the combined effect of these two drugs. By contrast, TA-5-Fu-BMN with the biphasic release profile

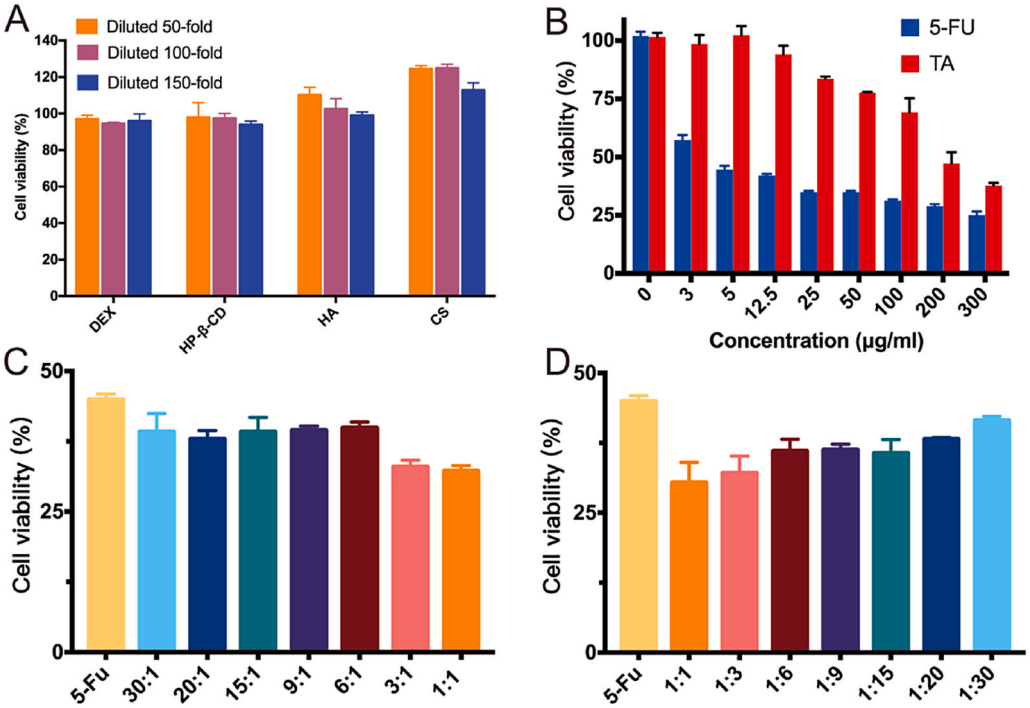

Fig. 5. Cytotoxicity of different excipients with varying concentrations in HSFb cells (A); Viability of HSFb cells treated by TA solutions, 5-Fu solutions (B), and TA-5-Fu solutions with various concentrations (C and D) for 24 h (mean ± SD, $n = 3$).

proposed in this study could control the release rate of 5-Fu due to the slow swelling process of CS and DEX in the skin, subsequently slowed down the clear rate of 5-Fu in the body. In particular, almost 50% of 5-Fu was retained in the HS after 24 h. Compared to TA Injection, both Tail layer@TA-5-Fu BMN and TA-5-Fu-BMN could prolong the TA retention time in HS tissue with similar profiles (marked as Tail layer@TA BMN and BMN@TA in Fig. S6). These results demonstrated that the proposed system ultimately prolonged the time that TA and 5-Fu coexist in the scar to improve the therapeutic efficiency.

3.6. Cytotoxicity of excipients on HS fibroblasts

The cell cytotoxicity test was used to assess the safety and biocompatibility of the excipients used for BMN preparation, including DEX, CS, HA, and HP-β-CD. The results showed that the cell viability of all groups was above 90% after diluting each excipient by 50, 100, and 150 times respectively, indicating that the excipients used in this study had good biocompatibility (Fig. 5A). In addition, the proliferation of HSFb cells was promoted with the increase in the concentration of CS and HA. This was because both HA and CS were polysaccharide compounds, which might act as nutrients to promote cell proliferation.

3.7. Proliferation inhibition of fibroblasts

HS is a chronic skin disease characterized by excessive fibroblasts proliferation. HSFb cells have a variety of malignant features including excessive proliferation, anti-apoptosis, excessive deposition, and altered collagen morphology. Therefore, inhibiting the HSFb cell proliferation is an effective strategy for HS treatment. The inhibitory effect of 5-Fu, TA, and their combination on HSFb cells was investigated. The results revealed that after incubated with different concentrations of 5-Fu for 24 h, cell viability decreased significantly compared to that of the control group (Fig. 5B). However, with further increase in 5-Fu concentration, cell viability showed a steady and gentle reduction. The cell viability of the TA group initially showed no decline, but when the concentration rose to 25.0 μg/mL, cell viability began to decrease as the

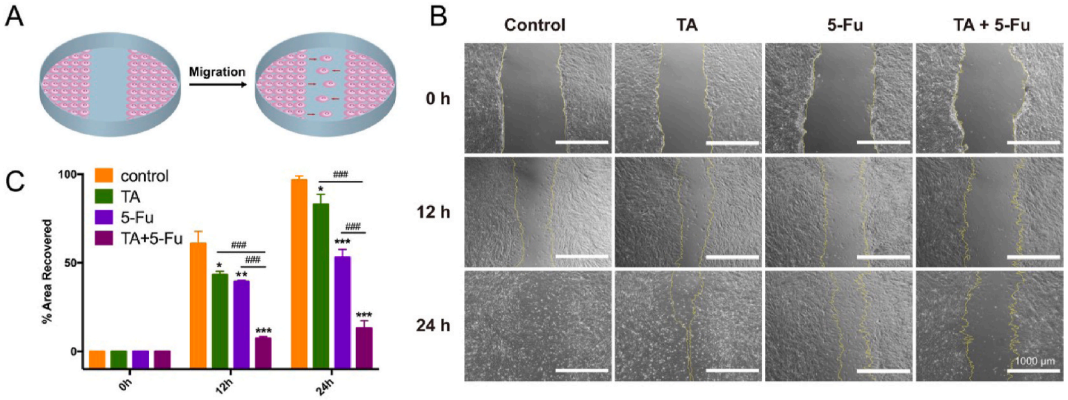

Fig. 6. Schematic illustration of the scratch wound model (A); Representative optical images showing the cells migrated toward wound gap (B) and the percentage of recovered area in scratch assay (C) (mean ± SD, $n = 3$). (*$p < 0.05$ & **$p < 0.01$ &***$p < 0.005$ vs. Control; #$p < 0.05$ & ##$p < 0.01$ & ###$p < 0.005$ vs. TA+5-Fu).

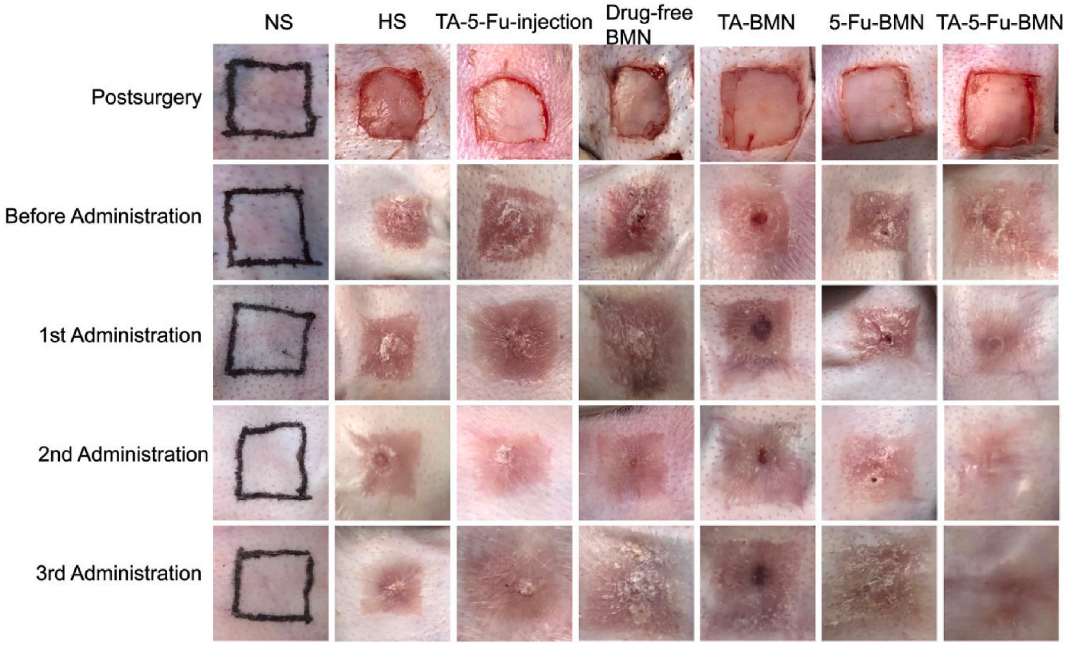

Fig. 7. Pictures of HS before and after administration of various preparations.

concentration increased. The half-maximal inhibitory concentrations (IC50 values) for 5-Fu and TA were found to be 4.0 μg/mL and 189.0 μg/mL, respectively. These results demonstrated that 5-Fu significantly inhibited the proliferation of fibroblasts, while the inhibition caused by TA appeared at higher concentrations.

Since the action mechanism of TA and 5-Fu was different, the combination of these two drugs may lead to better therapeutic efficacy. Therefore, we further evaluated the inhibition effect of TA in combination with 5-Fu on HSFb cells and optimized the proportion of these two drugs. Under the condition in which the 5-Fu concentration performed as a constant (5.0 μg/mL), when the ratio of TA to 5-Fu varied from 30:1 to 1:1, the cell viability decreased compared to the 5-Fu group (Fig. 5C and D). Whereas, the cell viability increased when the ratio of TA to 5-Fu varied from 1:1 to 1:30. The most significant synergistic effect occurred at the ratio of 1:1 with the lowest drug concentration. After linear regression by SPSS, the CI50 value calculated by equation (2) was 0.05, which was much less than 1, and indicated that the combination of TA and 5-Fu synergized the efficacy of proliferation inhibition.

3.8. Wound healing and cell migration

As a simple and economical method, *in vitro* wound scratch assay was performed to assess inhibition on the migration of fibroblasts (Fig. 6A). As shown in Fig. 6B and C, the healing rate of the control group reached 60.8% at 12 h, and the area of the scratch was almost covered by HSFb cells at 24 h, which revealed that the growth rate of HSFb cells was quite fast. Considering that excessive proliferation and migration of fibroblasts could result in HS, it is important to inhibit the migration of HSFb cells. The results showed that the scratch treated by TA alone almost recovered after 24 h, and the healing rate also reached 53.0% after treated by 5-Fu alone at 24 h. By contrast, only approximately 13.1% of the scratched area was recovered after treatment with the combination of TA and 5-Fu at 24 h. These results revealed that the combination of TA and 5-Fu significantly inhibited the migration of fibroblasts from forming HS tissue.

3.9. Inhibitory efficacy of hypertrophic scar

In this study, the HS model on rabbit ears was constructed to

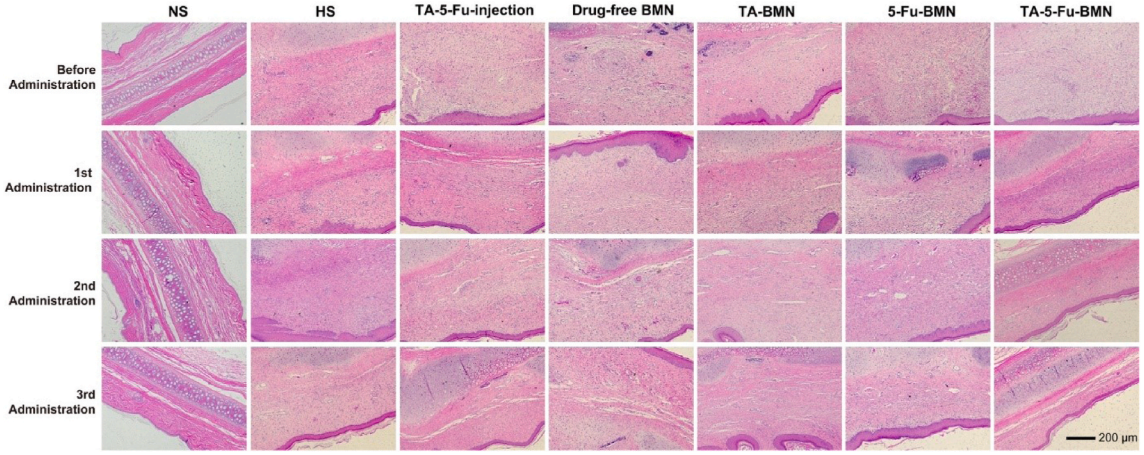

Fig. 8. Representative microscope histological pictures of HS stained by H&E before and after various treatments.

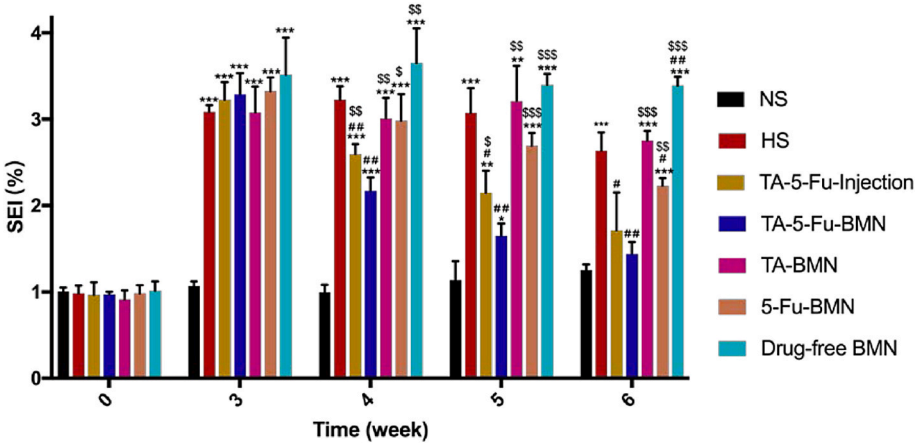

Fig. 9. SEI value of HS after various treatments (mean ± SD, $n = 3$). *$p < 0.05$ vs NS; **$p < 0.01$ vs NS; ***$p < 0.001$ vs NS; #$p < 0.05$ vs HS; ##$p < 0.01$ vs HS; ###$p < 0.001$ vs HS. $$p < 0.05$ vs TA-5-Fu-BMN; $$$p < 0.01$ vs TA-5-Fu-BMN; $$$$p < 0.001$ vs TA-5-Fu-BMN.

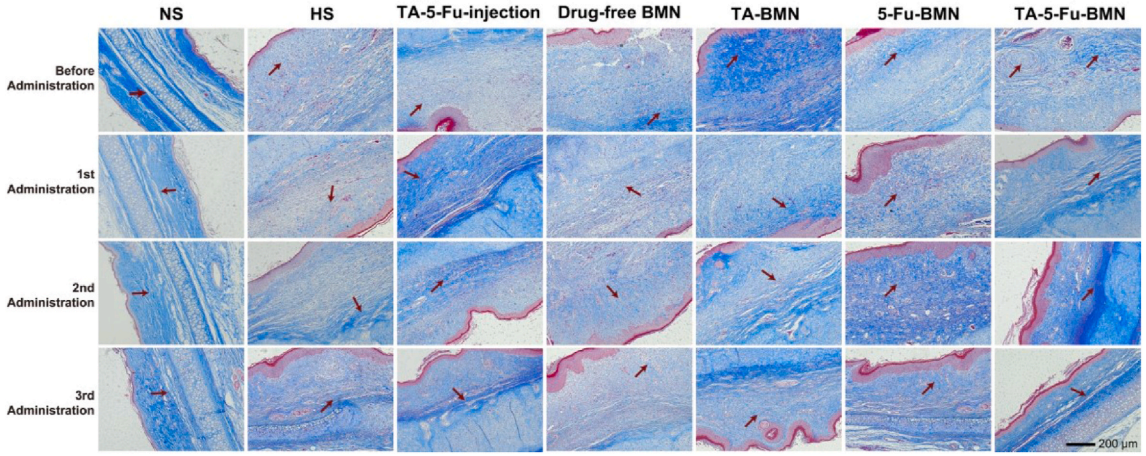

Fig. 10. Masson's trichrome staining of HS before and after various treatments.

investigate the inhibitory effect of TA-5-Fu-BMN *in vivo*. All wounds were re-epithelialized on the 14th day after skin resection and the HS tissues were finally formed. The appearance of the HS is shown in Fig. 7, which had a typical characteristic of HS with dark-red color and raised scar surface. The results showed that the redness of the scar received TA-5-Fu-BMN was eliminated significantly after three times administrations. By contrast, the scars still appeared reddish and firm in the texture of other groups, including the negative control group, injection group, drug-free BMN group, TA-BMN group, and 5-Fu-BMN group. Moreover, the scar of the TA-5-Fu-BMN group was observed to be smoother than other groups, and the border of the scar was more blurred. Therefore, the morphological observation indicated that the TA-5-Fu-BMN was effective in treating HS.

3.10. Histological analysis

Given that excessive proliferation of fibroblasts was contributed to the formation of HS, H&E staining displayed in Fig. 8was conducted to indicate the fibroblasts distribution at the HS tissue. The results showed that the dermis of normal skin appeared thin and arranged in order. On the contrary, the epidermis and dermis of HS were extremely epithelialized with fibroblasts arranged in disorder. Nodule and spiral structure formed by collagen was also observed in the scar tissue. After the third administration, the thickness of the epidermis and dermis treated with TA-5-Fu-BMN was similar to the normal skin, and the fibroblasts restored parallel and regular arrangement, while the fibroblasts still arranged irregularly in other groups. The cartilage still thickened to an extent, which might arise from the damage during modeling. Furthermore, the scar elevation index (SEI) was applied in an attempt to quantify the improvement in the HS, with smaller SEI representing less HS formation [38]. The SEI of each group was calculated at week 3, 4, and 5 after the operation, and the results were shown in Fig. 9. After the third administration, the SEI value of the TA-5-Fu-BMN group was 1.29 versus 2.53 of the HS group, which was significantly reduced ($p < 0.01$).

Besides, another important sign of HS formation is excessive collagen deposition. We assessed the accumulation of collagen fibers by Masson's trichrome staining. In Masson's trichrome stained tissues, the collagen fibers were shown as blue, while the muscular fibers were shown as red. As shown in Fig. 10, the blue collagen fibers of HS tissues were irregularly arranged with high density as compared with normal skin. After receiving the third administration of TA-5-Fu-BMN, the collagen fibers rearranged regularly and their density decreased, whereas large amounts of collagen fibers still appeared irregularly in other groups. All these results demonstrated that TA combined with 5-Fu in BMN was capable of suppressing the abnormal fibroblasts proliferation and collagen fibers deposition.

3.11. mRNA expressions of Col I and TGF-β1

Col I and TGF-β1 were found to be overexpressed in scar skin, which is closely related to scar formation. The vital factors of reducing scar

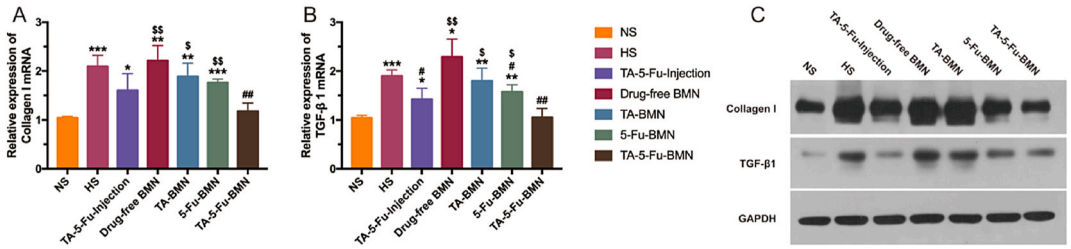

Fig. 11. Relative mRNA expressions of Col I (A) and TGF-β1 (B) and the relevant protein expressions (C) in HS tissues after the third administration with different formulations (mean ± SD, $n = 3$). *$p < 0.05$ vs NS; **$p < 0.01$ vs NS; ***$p < 0.001$ vs NS; #$p < 0.05$ vs HS; ##$p < 0.01$ vs HS; ###$p < 0.001$ vs HS; $$p < 0.05$ vs TA-5-Fu-BMN; $$$p < 0.01$ vs TA-5-Fu-BMN; $$$$p < 0.001$ vs TA-5-Fu-BMN.

formation include the sufficient inhibition of the excessive deposition of Col I and the TGF-β1 in the wound site. The mRNA expression level of TGF-β1 and Col I can further reflect the healing effect of scar, which was analyzed by RT-qPCR after the third administration. The results in Fig. 11A and B showed that the expression level of both Col I and TGF-β1 mRNA significantly increased in HS, which was twice as high as that of normal skin, indicating that HS was still in the active period. In contrast, the mRNA expression in HS treated with various drug loaded samples all decreased to some extent. In particular, TA-5-Fu-injection group and TA-5-Fu-BMN group revealed a significant decrease, with the mRNA expressions of TA-5-Fu-BMN group ameliorated to the basal level. The reason for the different performance of injection and BMN was that the biphasic release BMN designed in this study could realize sustained release of 5-Fu, subsequently improve the retention of the two drugs in the HS skin and ultimately strengthen the treatment efficacy.

3.12. Protein expressions of Col I and TGF-β1

Recent studies have suggested that the protein expression level of Col I and TGF-β1 could well reflect the healing process of HS [18]. The protein expression levels of Col I and TGF-β1 in different groups were measured by western blotting. As illustrated in Fig. 11C, compared with the normal skin, the significantly increased expression of both Col I and TGF-β1 in HS were confirmed. And the drug-free BMN group showed similar expression of Col I and TGF-β1 with the HS group, which indicated the negligible effect of BMN on HS treatment. Although TGF-β1 over-expression was significantly restrained both in the TA-5-Fu-Injection group and TA-5-Fu-BMN group, the TA-5-Fu-BMN group showed a better inhibitory effect on the expression of Col I. The above results demonstrated the superior therapeutic efficacy of TA-5-Fu-BMN on HS.

4. Conclusions

This study was aimed to design an ideal bilayer dissolving microneedle co-delivery system for HS treatment. The biphasic release behaviors consisted of rapid release TA from needle tail layer and sustained-release 5-Fu from needle tip layer were successfully realized. The obtained BMN could increase the retention time of TA and 5-Fu in the HS tissue for a better synergistic effect. The HS model in New Zealand rabbits was established to evaluate the HS treatment efficacy. The results of histological analysis, RT-qPCR detection, and Western blotting revealed the superior therapeutic effect of TA-5-Fu-BMN. In conclusion, the proposed bilayer dissolving microneedle offers an excellent alternative strategy for clinical treatment of HS in a sustained and minimally invasive manner.

Author contributions

Beibei Yang performed the majority of the experiments and wrote the manuscript. Yating Dong and Yifeng Shen helped to establish the animal model and actively engaged in the cell experiment and animal experiment. Ailin Hou helped to fabricate the microneedles. Guilan Quan revised the whole manuscript critically. Xin Pan and Chuanbin Wu designed the overall project and supervised the whole work.

CRediT authorship contribution statement

Beibei Yang: Conceptualization, Methodology, Validation, Formal analysis, Investigation, Writing - original draft, Visualization. **Yating Dong:** Investigation, Writing - review & editing. **Yifeng Shen:** Investigation. **Ailin Hou:** Investigation. **Guilan Quan:** Writing - review & editing, Funding acquisition. **Xin Pan:** Conceptualization, Supervision, Project administration. **Chuanbin Wu:** Conceptualization, Supervision, Project administration, Funding acquisition.

Declaration of competing interest

The authors declare no competing financial interest.

Acknowledgment

This work was supported by the National Natural Science Foundation of China [grant No. 81803466], the Research and Development Plan for Key Areas in Guangdong Province [grant No. 2019B020204002], and the National Science and Technology Major Program [grant No. 2017zx09101001].

Appendix A. Supplementary data

Supplementary data to this article can be found online at https://doi.org/10.1016/j.bioactmat.2021.01.014.

References

[1] L. Wang, J. Yang, B. Ran, X. Yang, W. Zheng, Y. Long, X. Jiang, Small molecular TGF-beta1-inhibitor-loaded electrospun fibrous scaffolds for preventing hypertrophic scars, ACS Appl. Mater. Interfaces 9 (38) (2017) 32545–32553.
[2] W. Weng, S. He, H. Song, X. Li, L. Cao, Y. Hu, J. Cui, Q. Zhou, H. Peng, J. Su, Aligned carbon nanotubes reduce hypertrophic scar via regulating cell behavior, ACS Nano 12 (8) (2018) 7601–7612.
[3] J.W. Lawrence, S.T. Mason, K. Schomer, M.B. Klein, Epidemiology and impact of scarring after burn injury: a systematic review of the literature, J. Burn Care Res. 33 (1) (2012) 136–146.
[4] J. Park, Y.C. Kim, Topical delivery of 5-fluorouracil-loaded carboxymethyl chitosan nanoparticles using microneedles for keloid treatment, Drug Deliv. Transl. Res. 11 (1) (2021) 205–213.
[5] Y. Ren, X. Zhou, Z. Wei, W. Lin, B. Fan, S. Feng, Efficacy and safety of triamcinolone acetonide alone and in combination with 5-fluorouracil for treating hypertrophic scars and keloids: a systematic review and meta-analysis, Int. Wound J. 14 (3) (2017) 480–487.
[6] Z. Zhang, Y. Liu, Y. Chen, L. Li, P. Lan, D. He, J. Song, Y. Zhang, Transdermal delivery of 5-aminolevulinic acid by nanoethosome gels for photodynamic therapy of hypertrophic scars, ACS Appl. Mater. Interfaces 11 (4) (2019) 3704–3714.
[7] M. Gholipourmalekabadi, S. Khosravimelal, Z. Nokhbedehghan, M. Sameni, V. Jajarmi, A.M. Urbanska, H. Mirzaei, M. Salimi, N.P.S. Chauhan, M. Mobaraki, R. L. Reis, A. Samadikuchaksaraei, S.C. Kundu, Modulation of hypertrophic scar formation using amniotic membrane/electrospun silk fibroin bilayer membrane in a rabbit ear model, ACS Biomater. Sci. Eng. 5 (3) (2019) 1487–1496.

[8] C.H. Hu, Y.W. Tseng, C.Y. Chiou, K.C. Lan, C.H. Chou, C.S. Tai, H.D. Huang, C. W. Hu, K.H. Liao, S.S. Chuang, J.Y. Yang, O.K. Lee, Bone marrow concentrate-induced mesenchymal stem cell conditioned medium facilitates wound healing and prevents hypertrophic scar formation in a rabbit ear model, Stem Cell Res. Ther. 10 (1) (2019) 275.
[9] C.C. Finnerty, M.G. Jeschke, L.K. Branski, J.P. Barret, P. Dziewulski, D.N. Herndon, Hypertrophic scarring: the greatest unmet challenge after burn injury, Lancet 388 (2016) 1427–1436, 10052.
[10] S. Monstrey, E. Middelkoop, J.J. Vranckx, F. Bassetto, U.E. Ziegler, S. Meaume, L. Teot, Updated scar management practical guidelines: non-invasive and invasive measures, J. Plast. Reconstr. Aesthetic Surg. 67 (8) (2014) 1017–1025.
[11] S. Lin, G. Quan, A. Hou, P. Yang, T. Peng, Y. Gu, W. Qin, R. Liu, X. Ma, X. Pan, H. Liu, L. Wang, C. Wu, Strategy for hypertrophic scar therapy: improved delivery of triamcinolone acetonide using mechanically robust tip-concentrated dissolving microneedle array, J. Contr. Release 306 (2019) 69–82.
[12] J.A. Ledon, J. Savas, K. Franca, A. Chacon, K. Nouri, Intralesional treatment for keloids and hypertrophic scars: a review, Dermatol. Surg. 39 (12) (2013) 1745–1757.
[13] Z. Bao, P. Gao, G. Xia, Z. Wang, M. Kong, C. Feng, X. Cheng, Y. Liu, X. Chen, A thermosensitive hydroxybutyl chitosan hydrogel as a potential co-delivery matrix for drugs on keloid inhibition, J. Mater. Chem. B 4 (22) (2016) 3936–3944.
[14] Y. Wo, Z. Zhang, Y. Zhang, Z. Zhang, K. Wang, X. Mao, W. Su, K. Li, D. Cui, J. Chen, Enhanced in vivo delivery of 5-fluorouracil by ethosomal gels in rabbit ear hypertrophic scar model, Int. J. Mol. Sci. 15 (12) (2014) 22786–22800.
[15] M.A. Khan, M.M. Bashir, F.A. Khan, Intralesional triamcinolone alone and in combination with 5-fluorouracil for the treatment of Keloid and Hypertrophic scars, JPMA (J. Pak. Med. Assoc.) 64 (9) (2014) 1003–1007.
[16] L. Huang, Y.J. Cai, I. Lung, B.C. Leung, A. Burd, A study of the combination of triamcinolone and 5-fluorouracil in modulating keloid fibroblasts in vitro, J. Plast. Reconstr. Aesthetic Surg. 66 (9) (2013) e251–e259.
[17] C.W.X. Tan, W.D. Tan, R. Srivastava, A.P. Yow, D.W.K. Wong, H.L. Tey, Dissolving triamcinolone-embedded microneedles for the treatment of keloids: a single-blinded intra-individual controlled clinical trial, Dermatol. Ther. 9 (3) (2019) 601–611.
[18] Z.Y. Jiang, X.C. Liao, M.Z. Liu, Z.H. Fu, D.H. Min, X.T. Yu, G.H. Guo, Efficacy and safety of intralesional triamcinolone versus combination of triamcinolone with 5-fluorouracil in the treatment of keloids and hypertrophic scars: a systematic review and meta-analysis, Aesthetic Plast. Surg. 44 (5) (2020) 1859–1868.
[19] R.B. Diasio, B.E. Harris, Clinical pharmacology of 5-fluorouracil, Clin. Pharmacokinet. 16 (4) (1989) 215–237.
[20] A. Than, C. Liu, H. Chang, P.K. Duong, C.M.G. Cheung, C. Xu, X. Wang, P. Chen, Self-implantable double-layered micro-drug-reservoirs for efficient and controlled ocular drug delivery, Nat. Commun. 9 (1) (2018) 4433.
[21] Y. Hao, Y. Chen, X. He, F. Yang, R. Han, C. Yang, W. Li, Z. Qian, Near-infrared responsive 5-fluorouracil and indocyanine green loaded MPEG-PCL nanoparticle integrated with dissolvable microneedle for skin cancer therapy, Bioact. Mater. 5 (3) (2020) 542–552.
[22] Y. Xie, H. Wang, J. Mao, Y. Li, M. Hussain, J. Zhu, Y. Li, L. Zhang, J. Tao, J. Zhu, Enhanced in vitro efficacy for inhibiting hypertrophic scar by bleomycin-loaded dissolving hyaluronic acid microneedles, J. Mater. Chem. B 7 (42) (2019) 6604–6611.
[23] J. Chi, X. Zhang, C. Chen, C. Shao, Y. Zhao, Y. Wang, Antibacterial and angiogenic chitosan microneedle array patch for promoting wound healing, Bioact. Mater. 5 (2) (2020) 253–259.
[24] W. Li, R.N. Terry, J. Tang, M.R. Feng, S.P. Schwendeman, M.R. Prausnitz, Rapidly separable microneedle patch for the sustained release of a contraceptive, Nat. Biomed. Eng. 3 (3) (2019) 220–229.
[25] K. Lee, H.B. Song, W. Cho, J.H. Kim, J.H. Kim, W. Ryu, Intracorneal injection of a detachable hybrid microneedle for sustained drug delivery, Acta Biomater. 80 (2018) 48–57.
[26] A.L. Hou, G.L. Quan, B.B. Yang, C. Lu, M.L. Chen, D. Yang, L.L. Wang, H. Liu, X. Pan, C.B. Wu, Rational design of rapidly separating dissolving microneedles for precise drug delivery by balancing the mechanical performance and disintegration rate, Adv. Healthc. Mater. 8 (21) (2019) 11.
[27] L.K. Vora, R.F. Donnelly, E. Larraneta, P. Gonzalez-Vazquez, R.R.S. Thakur, P. R. Vavia, Novel bilayer dissolving microneedle arrays with concentrated PLGA nano-microparticles for targeted intradermal delivery: proof of concept, J. Contr. Release 265 (2017) 93–101.
[28] Y. He, C. Hong, J. Li, M.T. Howard, Y. Li, M.E. Turvey, D. Uppu, J.R. Martin, K. Zhang, D.J. Irvine, P.T. Hammond, Synthetic charge-invertible polymer for rapid and complete implantation of layer-by-layer microneedle drug films for enhanced transdermal vaccination, ACS Nano 12 (10) (2018) 10272–10280.
[29] W.G. Bae, H. Ko, J.Y. So, H. Yi, C.H. Lee, D.H. Lee, Y. Ahn, S.H. Lee, K. Lee, J. Jun, H.H. Kim, N.L. Jeon, W. Jung, C.S. Song, T. Kim, Y.C. Kim, H.E. Jeong, Snake fang-inspired stamping patch for transdermal delivery of liquid formulations, Sci. Transl. Med. 11 (503) (2019).
[30] C. Dillon, H. Hughes, N.J. O'Reilly, P. McLoughlin, Formulation and characterisation of dissolving microneedles for the transdermal delivery of therapeutic peptides, Int. J. Pharm. 526 (1–2) (2017) 125–136.
[31] Q. Zhang, C. Xu, S. Lin, H. Zhou, G. Yao, H. Liu, L. Wang, X. Pan, G. Quan, C. Wu, Synergistic immunoreaction of acupuncture-like dissolving microneedles containing thymopentin at acupoints in immune-suppressed rats, Acta Pharm. Sin. B 8 (3) (2018) 449–457.
[32] M.C. Kearney, E. Caffarel-Salvador, S.J. Fallows, H.O. McCarthy, R.F. Donnelly, Microneedle-mediated delivery of donepezil: potential for improved treatment options in Alzheimer's disease, Eur. J. Pharm. Biopharm. 103 (2016) 43–50.
[33] M.C. Chen, M.H. Ling, K.Y. Lai, E. Pramudityo, Chitosan microneedle patches for sustained transdermal delivery of macromolecules, Biomacromolecules 13 (12) (2012) 4022–4031.
[34] C. Lee, H. Kim, S. Kim, S.F. Lahiji, N.Y. Ha, H. Yang, G. Kang, H.Y.T. Nguyen, Y. Kim, M.S. Choi, N.H. Cho, H. Jung, Comparative study of two droplet-based dissolving microneedle fabrication methods for skin vaccination, Adv. Healthc. Mater. 7 (11) (2018), e1701381.
[35] M. Dangol, S. Kim, C.G. Li, S. Fakhraei Lahiji, M. Jang, Y. Ma, I. Huh, H. Jung, Anti-obesity effect of a novel caffeine-loaded dissolving microneedle patch in high-fat diet-induced obese C57BL/6J mice, J. Contr. Release 265 (2017) 41–47.
[36] O. Kloeters, A. Tandara, T.A. Mustoe, Hypertrophic scar model in the rabbit ear: a reproducible model for studying scar tissue behavior with new observations on silicone gel sheeting for scar reduction, Wound Repair Regen. 15 (Suppl 1) (2007) S40–S45.
[37] D.D. Zhu, B.Z. Chen, M.C. He, X.D. Guo, Structural optimization of rapidly separating microneedles for efficient drug delivery, J. Ind. Eng. Chem. 51 (2017) 178–184.
[38] L. Cheng, X. Sun, X. Zhao, L. Wang, J. Yu, G. Pan, B. Li, H. Yang, Y. Zhang, W. Cui, Surface biofunctional drug-loaded electrospun fibrous scaffolds for comprehensive repairing hypertrophic scars, Biomaterials 83 (2016) 169–181.